The Journal of Experimental Biology 203, 1755–1765 (2000)
Printed in Great Britain © The Company of Biologists Limited 2000
JEB2630

HORIZONTAL FLIGHT OF A SWALLOW (*HIRUNDO RUSTICA*) OBSERVED IN A WIND TUNNEL, WITH A NEW METHOD FOR DIRECTLY MEASURING MECHANICAL POWER

C. J. PENNYCUICK[1], ANDERS HEDENSTRÖM[2,*] AND MIKAEL ROSÉN[2]

[1]*School of Biological Sciences, University of Bristol, Woodland Road, Bristol BS8 1UG, UK* and
[2]*Department of Animal Ecology, Lund University, Ecology Building, S-223 62 Lund, Sweden*

*Author for correspondence (e-mail: anders.hedenstrom@zooekol.lu.se)

Accepted 13 March; published on WWW 10 May 2000

Summary

A swallow flying in the Lund wind tunnel was observed from the side and from behind, by two synchronised high-speed video cameras. The side-view camera provided a record of the vertical position of a white mark, applied to the feathers behind and below the eye, from which the vertical acceleration was obtained. The rear-view camera provided measurements of the mean angle of the left and right humeri above horizontal. From these data, the force acting on the body, the moment applied by each pectoralis muscle to the humerus and the rotation of the humerus were estimated and used to analyse the time course of a number of variables, including the work done by the muscles in each wing beat. The average mechanical power turned out to be more than that predicted on the basis of current estimates of body drag coefficient and profile power ratio, possibly because the bird was not flying steadily in a minimum-drag configuration. We hope to develop the method further by correlating the mechanical measurements with observations of the vortex wake and to apply it to birds that have been conditioned to hold a constant position in the test section.

Key words: flight, mechanical power, wind tunnel, swallow, *Hirundo rustica.*

Introduction

The basic assumption of flight mechanics is that the rate at which the muscles have to do work in flight can be calculated from the physics of supporting the weight of the body against gravity, and of overcoming the drag of the body and wings. This rate of doing work is the mechanical power. The rate at which fuel energy is required (metabolic power) is determined primarily by the mechanical power, but the connection is not simple because the conversion of fuel energy into mechanical work depends on physiological processes for which no complete quantitative theory exists. Thus, to test a flight mechanical theory, it is necessary to measure the mechanical power directly (like the shaft power of an engine) as opposed to measuring the rate of consumption of fuel energy. Mechanical power was first measured directly by Biewener et al. (1992) on a starling flying in a wind tunnel, and the same method was used in a free-flight experiment on pigeons by Dial and Biewener (1993). They measured the force exerted by the pectoralis muscle during the downstroke by bonding a strain gauge to the upper surface of the deltoid crest of the humerus, in effect using distortion of the bone as a spring balance. The distance shortened by the muscle was estimated from video recordings and multiplied by the force to give the work done in each contraction. Multiplying this by the wingbeat frequency gave the power. ‘Force’ and ‘distance shortened’ are actually not definable in the pectoralis of a bird because the motion imparted to the humerus is rotary rather than linear, and different fibres in the muscle shorten through very different distances. Work estimates are, at best, proportional rather than equal to the actual work done. The shape of the power curve can be observed from proportional measurements (Biewener et al., 1992; Dial et al., 1997), as can the shape and timing of work loops (Biewener et al., 1998), but not the absolute value of the power, as required for comparison with values predicted from an aerodynamic model. In any case, insufficient information about the morphology of the bird, and the conditions of flight, was given in any of these projects to allow such predictions to be attempted from the data as published. Undesirable features of the technique are that surgery is required to implant sensors, and trailing wires have to be connected to the bird.

To measure the work done by the pectoralis muscle in rotating the humerus, the moment exerted by the muscle (rather than the force) has to be multiplied by the angle (rather than the distance) through which the humerus rotates. In this paper, we describe a new method for measuring those variables, and for estimating mechanical power, which does not require transducers to be implanted or wires to be connected to the bird. The principle of our method is to observe the motion of

the body and wings as the bird flies in the wind tunnel and then to apply Newton's laws of motion to deduce what forces are acting and how much work is being done. We compare the estimated power at different speeds with the power predicted from the theory of Pennycuick (1989a). This theory requires values to be assigned to a number of variables, some of which are difficult to measure and are poorly known. The discussion takes the form of searching for combinations of variable values that will give a satisfactory approximation to the observed results, and then considering the physical implications of the inferred values.

Materials and methods

Birds and wind tunnel

The experimental subject was one of two swallows (*Hirundo rustica*) captured as adults near Vomb, Sweden, on 21 May 1999, and released on 15 June 1999. After a period of habituation to captivity and handling, the swallows were introduced into the Lund wind tunnel, where they quickly learned to fly with minimal training. Full details of the layout and construction of this wind tunnel were given by Pennycuick et al. (1997), together with performance measurements. The width of the test section (1.20 m) was just under four times the wing span of the swallow (Table 1).

The swallow flew in the closed part of the test section, approximately 50 cm downstream of a fine net placed across the exit from the contraction. The thread diameter of the net was 0.15 mm, with a mesh size of 29 mm×29 mm, i.e. thinner threads and larger mesh than the net used in the performance tests described by Pennycuick et al. (1997). The Reynolds number of the threads would have been approximately 62 at $6\,m\,s^{-1}$, rising to 114 at $11\,m\,s^{-1}$. This is above the threshold (*Re*=40) at which threads generate no turbulence, and we therefore assume that the net introduced a small amount of turbulence into the flow. Later, we note the possibility that this could have had an effect on our results.

Primary observations

When any bird settles down in steady flapping flight in the wind tunnel, its body can be seen to oscillate up and down with each wing beat. We observed this motion, and also the wing beat itself, using two synchronised high-speed digital video cameras (Redlake Motionscope PCI 500) placed as shown in Fig. 1 to give simultaneous pictures of the bird from the side and from behind. The cameras were controlled by a Pentium II 233 MHz computer with Windows NT, running Version 2.15 of the Motionscope PCI application software of Redlake. The camera output was recorded initially in the form of two animation (.AVI) files, one from each camera. The individual frames were extracted from these in the form of sequences of compressed (.JPG) monochrome picture files, measuring 480 pixels×420 pixels. The pixels were square (aspect ratio 1).

The side-view camera was positioned 75 cm from the centre of the test section, and the zoom lens was adjusted so that the width of the picture was sufficient to accommodate the tip of the beak back to the posterior edge of the wing. The primary measurement from this camera was the *XY* position in pixels of a white spot made with typewriter correction fluid (Tippex) behind and below the eye. The spot was placed as far back as possible, without being momentarily hidden by the wing at mid-downstroke, so as to minimise the possibility that the spot might move vertically if the bird were to flex its neck at each wingbeat. Actually, neither swallows nor any other species so far observed in the Lund wind tunnel stabilised their heads, except when looking at a perch or the floor, when about to land. In steady flight, the head moved up and down with the body, with no measurable flexing of the neck or rotation of the beak, in all species including waders and ducks.

Table 1. *Body and wing measurements for the swallow*

Mass of whole body (kg)	0.0190
Estimated mass of wingless body (kg)	0.0159
Wing span (m)	0.318
Wing area (m^2)	0.0132
Estimated wing moment of inertia ($kg\,m^2$)	2.74×10^{-6}
Gliding moment arm (m)	0.0598

Wing moment of inertia was estimated from wing span according to Kirkpatrick (1990).

The rear-view camera was set up to accommodate the whole wing span at mid-downstroke, with some space for lateral movement. In each rear-view picture, the *XY* (pixel) positions of four points were first recorded, marking the ends of two straight lines, parallel to the left and right humeri. The angle between each humerus and horizontal was determined from the ends of the lines. The average value for the left and right humeri was our estimate of the 'humerus angle' ϕ, measured upwards from the horizontal position. The loading and manipulation of sequences of images were automated by writing an ARexx script to control the image processing program ImageFX (Nova Design Inc.) on a Commodore Amiga 3000 computer. This script also recorded the coordinates of points selected with the mouse, directly to the 'raw' data file. Subsequent processing of the files was also done on the Amiga, using programs written as required in Hisoft Basic 2.

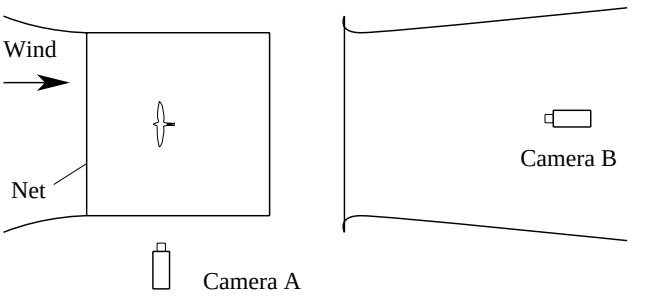

Fig. 1. The swallow flew in the closed part of the test section and was observed from the side by camera A and from behind by camera B. Full details of the wind tunnel were given by Pennycuick et al. (1997).

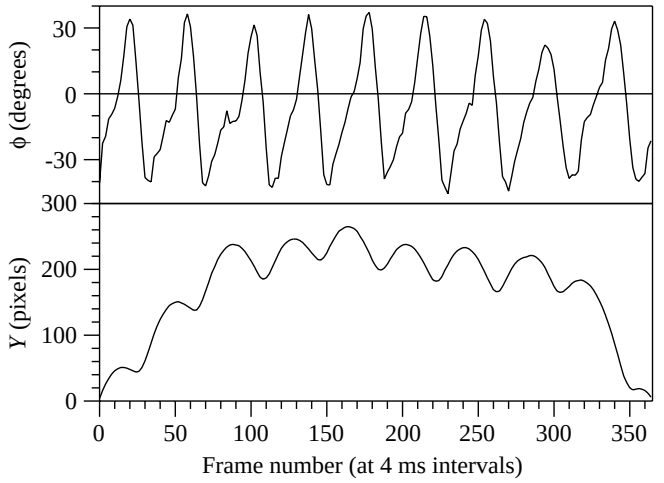

Fig. 2. Unfiltered data from sequence 'O'. Upper graph: humerus angle (ϕ), in degrees above horizontal, average for left and right wings. Lower graph: height of the white spot on the bird's head, in pixels above the bottom of the frame. Frame numbers run from 0 to 364. The height of the graph (300 pixels) is equivalent to approximately 80 mm vertically at the bird's position.

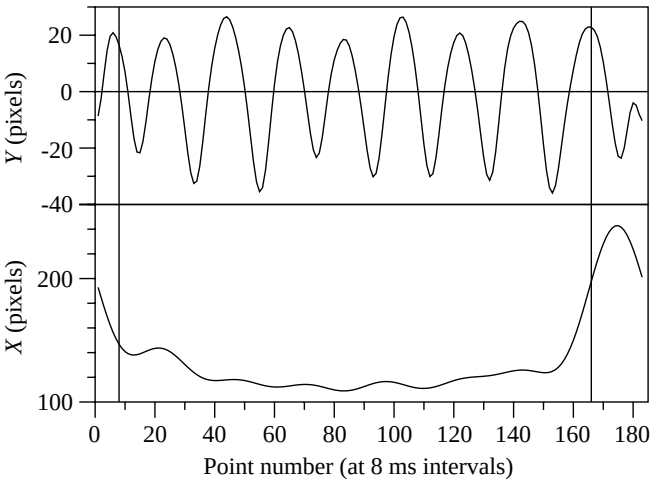

Fig. 3. Filtered data from sequence 'O'. Upper graph: height in pixels above the bottom of the frame, band-pass filtered from 4.10 to 21.9 Hz. Lower graph: distance in pixels from the left (upstream) edge of the frame, low-pass filtered from 0 to 4.78 Hz. Vertical lines mark the beginning and end of the measurement period. Point numbers run from 1 to 183, being derived from the even-numbered frames in Fig. 2. The height of the lower graph (160 pixels) is equivalent to approximately 42 mm horizontally.

Frequency filtering of data files

The three unfiltered data files for each sequence contained the following numbers for each frame: *X*, the distance in pixels from the left edge of frame; *Y*, the distance in pixels from the bottom edge of frame; and ϕ, the humerus angle in degrees above horizontal (average of left and right).

Fig. 2 shows an example of unfiltered *Y* and ϕ files from sequence 'O', which consisted of 365 frames, at intervals of 4 ms. The even-numbered frames were used to measure the 'raw' data points at intervals of 8 ms. The *Y* record shows a marked oscillatory component at the wingbeat frequency, superimposed on components at lower frequencies due to the bird moving up from the bottom of the frame and then back down again. The ϕ record shows some irregularities during the upstroke caused by difficulty in discerning the humerus position when the wing is strongly flexed.

In the subsequent processing, *X* and *Y* were converted into *x* and *y*, the corresponding distances from the left and bottom edges of the frame, respectively (in metres). The scale, which varied slightly as the bird wandered towards or away from the camera, was obtained by measuring the apparent distance (in pixels) between the white spot behind and below the eye and a second white mark near the tip of the bill. This was done for every eighth frame, rejecting frames in which the distal spot was out of the picture or in which the swallow had turned its head to the side, so shortening the apparent distance between the two spots. Such gaps were filled by linear interpolation or by holding the scale constant if frames were missing at the beginning or end of the sequence.

The power calculation required the first derivative of *x* (horizontal velocity), the second derivative of *y* (upward acceleration) and the value and first derivative of ϕ (angular position and velocity respectively). Derivatives can be obtained from a time series by comparing each measurement with the previous one, but this process is very sensitive to small irregularities caused by the limited resolution of measurement (±1 pixel, in our case). Before extracting the derivatives, we had to smooth the data. First, we applied a Fourier transform to the original time series using the formulae given by Chatfield (1996). This transforms the data from the 'time domain' to the 'frequency domain', representing the original time series as the sum of a series of sine waves of different frequencies, each with its own amplitude and phase. When added back together, these frequency components recreate the original time series. If some frequency components are omitted, a 'filtered' time series results. Fig. 3 shows an example of filtered *X* and *Y* files from a picture sequence at an equivalent air speed of 10 m s^{-1} (sequence 'O'; see Table 2). The filtered ϕ file from the same sequence is shown later (see Fig. 9). Different filtering was used on the three files, as follows.

The *x* file was 'low-pass' filtered to include only frequencies from zero to 0.8 times the wingbeat frequency. The filtered file was used to estimate any change in the bird's air speed between the beginning and end of the series, thus allowing for any kinetic energy change when computing the average power. It looks much the same as the unfiltered *x* file (not shown), except that minor fluctuations at higher frequencies, which would have caused spurious variations of speed, have been filtered out.

In the case of the *y* file, we wanted to know the acceleration that occurs within each wing beat, but not the slow changes as the bird wanders up and down the frame. We used 'band-pass' filtration for this, retaining frequencies between 0.7 and 3.5 times the wingbeat frequency, but rejecting those above and

below this band. The high-frequency cutoff smoothes the curve, making extraction of the second derivative practicable, while the low-frequency cutoff eliminates slow movements up and down. The component at zero frequency is the baseline. By removing it, the original record, which runs upwards from zero, is changed into a record that oscillates above and below a new zero line.

In the case of the humerus angle, we needed to know the absolute value relative to the original zero line (horizontal). We smoothed this series by low-pass filtration, retaining frequencies from zero to 3.5 times the wing-beat frequency, but removing the 'wrinkles' at higher frequencies.

The lowest frequency in the Fourier series is determined by the length of the series, and the highest is half the sample frequency. The Fourier transform does not identify the wingbeat frequency. We did that in advance of the filtering operation by noting the frame numbers at which the wing passed upwards and downwards through the zero (horizontal) position.

Estimating velocity and acceleration

We read the values from the filtered x, y and ϕ files sequentially, and estimated derivatives from a moving group of three successive values. Denoting the most recently read value of y as y_2, the previous value as y_1 and the one before that as y_0, we estimated the upward velocity (v_y) as the average of the velocities in the intervals before and after the time of y_1:

$$v_y = [c(y_2 - y_0)]/(2\Delta t)\,, \tag{1}$$

c being the scale factor for converting distances (pixels to metres) and Δt the interval between succcessive observations of y (8 ms). This estimate refers to the time of the middle value of the three, y_1. The angular velocity of the humerus (ω) was found in the same manner from three successive observations of ϕ. The upward acceleration (a_y) was found from the difference in the velocities before and after the time of y_1:

$$a_y = c(y_2 - 2y_1 + y_0)/\Delta t^2\,. \tag{2}$$

The subsequent calculations refer to the time of y_1 and require data to have been read for at least one frame before and one frame after y_1. Data were read sequentially from the beginning of the file, but calculations were only carried out during a 'measurement interval', which covered a whole number of wingbeat cycles, starting and ending at the frame immediately following an upward transition of the humerus angle through the horizontal position.

Upward force at the shoulders

To estimate the upward force applied by the wings to the body from the acceleration, we used an empirical formula from Kirkpatrick (1990) for the mass of one wing (m_w) as a function of the total body mass (m):

$$m_w = (9.74\times10^{-2})m^{1.10}\,. \tag{3a}$$

We inverted this to give the mass of the wingless body (m_b), after subtracting the estimated mass of both wings from the total mass:

$$m_b = m - (0.195m^{1.1})\,. \tag{3b}$$

Our estimate for m_b was 15.9 g, or 84 % of the total body mass, very close to a measured value of 85 % for a dead swallow from the freezer. Kirkpatrick's exponent of 1.1 expresses a general scaling relationship whereby, at larger sizes, structure mass is a higher fraction of the whole (Spedding and Lissaman, 1998).

If the upward acceleration (a_y) has been determined, then the upward force F_b, applied by the wings to the body at the shoulder joints, follows from Newton's second law of motion:

$$F_b = m_b(a_y + \boldsymbol{g})\,, \tag{4}$$

where $\boldsymbol{g}$ is the acceleration due to gravity. This force does positive work as the body moves upwards and negative work as it moves down, but this is not a direct measure of the work done by the muscles. If integrated over a complete wingbeat cycle, the work equates to the gain in potential energy (ΔE_p) during the cycle, thus:

$$\Delta E_p = m_b\boldsymbol{g}(y_2 - y_1)\,, \tag{5}$$

where y_1 and y_2 are the y positions at the beginning and end of the cycle, respectively. If the bird begins and ends the cycle at the same height, the potential energy gain is zero. The potential energy gain was calculated for each sequence as a correction to the estimated work done by the flight muscles. This correction could be either positive or negative, but was always small because of the limited height of the field of view of the camera at the position of the bird (approximately 11 cm).

Estimating the moment applied to the humerus

During the downstroke, the pectoralis muscle does work by applying a downward moment to the humerus, and shortening. We estimated the moment from the balance of forces on one wing, shown at a point during the downstroke in Fig. 4. The upward force (F_u), applied by one wing to the shoulder joint, is half of the force found from the upward acceleration in equation 4:

$$F_u = F_b/2\,, \tag{6}$$

and this has to be balanced by the vertical component of the lift force (L), which acts perpendicularly to the surface of the wing. The horizontal components of the lift forces on the left and right wings balance one another and cancel. The lift force on one wing is therefore:

$$L = F_u/\cos\phi\,, \tag{7}$$

where ϕ is the humerus angle measured upwards from the horizontal position. This force applies a moment (M) about the shoulder joint, where

$$M = LA\,. \tag{8}$$

The moment arm (A) was estimated as shown in Fig. 5, which is a tracing of the swallow's left wing with the joints fully extended in the manner prescribed by Pennycuick (1999). The wing outline was divided into 15 chordwise strips, each 10 mm wide in the spanwise direction. The area of each strip was

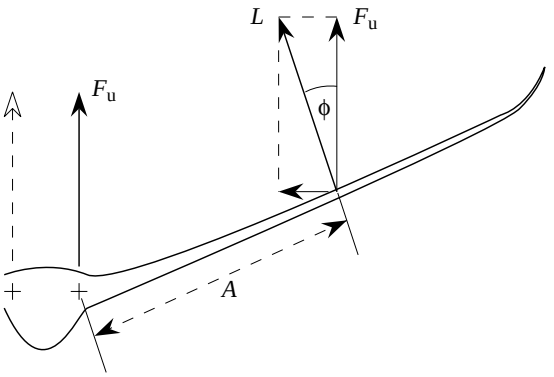

Fig. 4. Relationship at a point during the downstroke between the vertical force on one shoulder joint (F_u), the lift force on the wing (L) and the humerus angle (ϕ). F_u is half the upward force on the body (F_b), determined from the upward acceleration (equation 6). The moment applied by the pectoralis muscle to the humerus is found by multiplying the lift force by the moment arm (A).

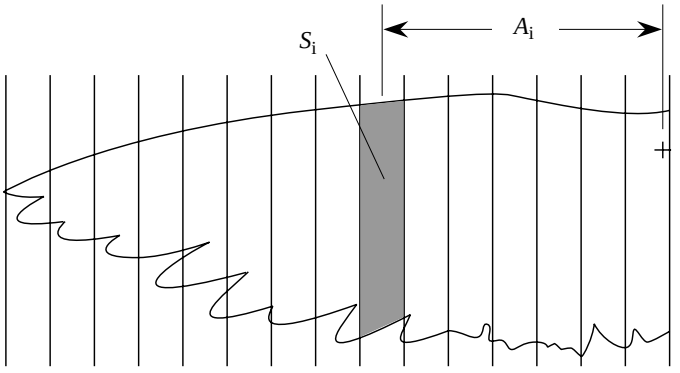

Fig. 5. Strip analysis for calculating the moment arm. S_i is the area of strip i, and A_i is its moment arm about the shoulder joint (cross).

measured, and also its distance from the estimated position of the shoulder joint. Denoting the area of strip i as S_i, and its moment arm as A_i, the force (F_i) developed on that strip depends not only on the forward speed (V) but also on the downward speed due to the flapping motion, which is ωA_i, where ω is the angular velocity of the wing about the shoulder joint:

$$F_i = (\rho C_L/2)S_i(V^2 + A_i^2\omega^2)\,, \quad (9)$$

where C_L is the lift coefficient and ρ is the air density. The moment (M_i) exerted by the force on the strip about the shoulder joint is found by multiplying the force by the moment arm (A_i), measured for that strip:

$$M_i = (\rho C_L/2)S_iA_i(V^2 + A_i^2\omega^2)\,. \quad (10)$$

The mean moment arm A for the wing as a whole is found by dividing the total moment, obtained by summing all the strips, by the total force:

$$A = \sum S_iA_i(V^2 + A_i^2\omega^2)/\sum S_i(V^2 + A_i^2\omega^2)\,. \quad (11)$$

This method of finding the mean moment arm implies that the lift coefficient is constant along the wing span, but does not require its value to be known. On the contrary, since the lift force (L) has been determined from the acceleration record, the lift coefficient can be estimated by inverting equation 9 and summing over all the strips:

$$C_L = 2L/[\rho\sum S_i(V^2 + A_i^2\omega^2)]\,. \quad (12)$$

Table 2. *Summary of data*

Sequence	EAS ($m\,s^{-1}$)	Frames at 4 ms intervals	Number of wingbeat cycles	Measurement interval (s)	Frequency (Hz)
I	11.0	0–234	5	0.752	6.65
J	11.0	0–372	10	1.42	7.06
K	11.0	0–300	8	1.14	7.04
L	8.0	0–600	15	2.16	6.94
M	8.0	0–820	23	3.08	7.47
N	10.0	0–466	11	1.54	7.16
O	10.0	0–364	8	1.26	6.33
P	10.0	0–250	6	0.880	6.82
Q	6.0	0–408	9	1.10	8.15
R	6.0	0–304	5	0.680	7.35

EAS, equivalent air speed.

Power and work

Having found the lift force from equation 7 and the moment arm from equation 11, the moment applied by the pectoralis muscle to the humerus (equation 8) can be estimated for each frame. Multiplying this moment by the downward angular velocity gives the instantaneous power. Multiplying this by the time interval (Δt) between frames gives the increment of work done (ΔQ):

$$\Delta Q = LA\omega\Delta t\,. \quad (13)$$

These increments were accumulated to find the total work done during the downstroke (but not during the upstroke; see below). The average power over several complete wingbeat cycles was found by summing the work done by the muscles of both sides during the downstrokes and dividing by the time for the full cycle. The beginning and end points of each cycle were defined by the transition from negative to positive humerus angle (middle of the upstroke) so as to ensure that the whole downstroke fell within one cycle.

Results

The data consisted of 10 picture sequences taken during a single experimental session on 7 June 1999 at four values of the equivalent air speed, 6, 8, 10 and 11 $m\,s^{-1}$ (Table 2). The air density was just below the standard sea level value of 1.23 $kg\,m^{-3}$ (Table 3), meaning that the true air speed was approximately 1 % faster than the equivalent air speed. The distinction is insignificant for our results, but it would be significant at certain points in the calculation (noted), in other wind tunnels, situated at higher elevations. The principle is

Table 3. *Air conditions measured during the experimental session*

Barometric pressure (hPa)	1015–1017
Air temperature (°C)	18.9–21.2
Air density (kg m^{-3})	1.19–1.21
$\sqrt{\sigma}$	0.987–0.991

σ is the ratio of air density to the sea level value, and $\sqrt{\sigma}$ is the conversion factor between true and equivalent air speed.

explained in aeronautical textbooks, and practical formulae are given by Pennycuick (1999).

Wing kinematics

At all speeds, the wing was extended fully during the downstroke. It was shortened by flexing the elbow and wrist joints during the upstroke, to a greater extent at higher speeds. As the humerus started to rise from the bottom of the downstroke, the lift force collapsed and the primary feathers lost their upward curvature. Flexure of the carpal joint caused the hand-wing to continue apparently rotating downwards (as seen by the rear-view camera) as the humerus started to rise. The wing folded to its minimum span as it came up towards the level position. At the higher speeds, there was often a perceptible pause just before the level position, visible in several cycles of Fig. 2. This 'upstroke pause' was seen at 10 and 11 m s^{-1}, but not at 6 or 8 m s^{-1}. From this point, the wing was progressively extended until it reached the fully up position, when extension was completed, and the primary feathers re-developed their upward curvature.

In the case of variables that could be estimated separately in each wingbeat cycle, a mean value could be found for the whole sequence, together with a standard deviation. The longest mean wingbeat period (i.e. lowest mean frequency) was not seen at low speeds, as reported in two other species by Pennycuick et al. (1996), but at around 10 m s^{-1} (Fig. 6). The decrease of wingbeat frequency at higher speeds (10 and 11 m s^{-1}) appears to be due to the 'upstroke pause' seen in the graphs of humerus angle in Figs 2 and 9, which was not seen at speeds below 10 m s^{-1}. The downstroke fraction, i.e. the time for the downstroke expressed as a fraction of the total wingbeat period, decreased with speed (Fig. 6). The magnitude of the (negative) angular velocity during the downstroke increased progressively throughout the speed range (Fig. 7), as did the top-to-bottom angular swing of the humerus (Fig. 7).

Span ratio and force ratio

In Fig. 8, the average upward acceleration during the downstroke, and also during the upstroke, is plotted for the 10 sequences against equivalent air speed. As above, zero acceleration means that the bird feels normal gravity, while an acceleration of $-1\boldsymbol{g}$ means that it is in free fall, with no upward force applied by the wings to the body. The average acceleration can be related to wing kinematics. It was noted above that the wing span was reduced during the upstroke, at all speeds, by flexure of the elbow and wrist joints, and this

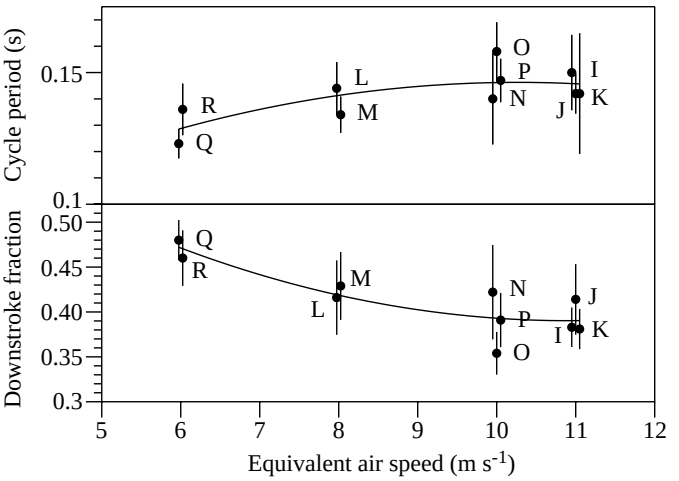

Fig. 6. Upper graph: wingbeat period in the 10 sequences I–R, plotted against equivalent air speed. Lower graph: downstroke time as a fraction of total wingbeat period. The points and error bars represent the means and standard deviations of estimates from the individual wing beats within each sequence. Points at the same speed have been offset to show the error bars. The fitted curves are second-degree polynomials, but these have no formal significance.

can be expressed as the 'span ratio'. The apparent distance (in pixels) between the left and right wing tips was measured in rear-view pictures, on each frame where the humerus passed downwards through the wings-level position, and again on the next frame in which the humerus passed upwards through the level position. The span ratio was estimated from each pair of frames as the ratio of the span in the upstroke to that in the downstroke. This ratio is plotted, with standard deviation bars, in Fig. 8. It declined from a value near 0.5 at 6 m s^{-1} to approximately 0.3 at 10 and 11 m s^{-1}. According to the notion

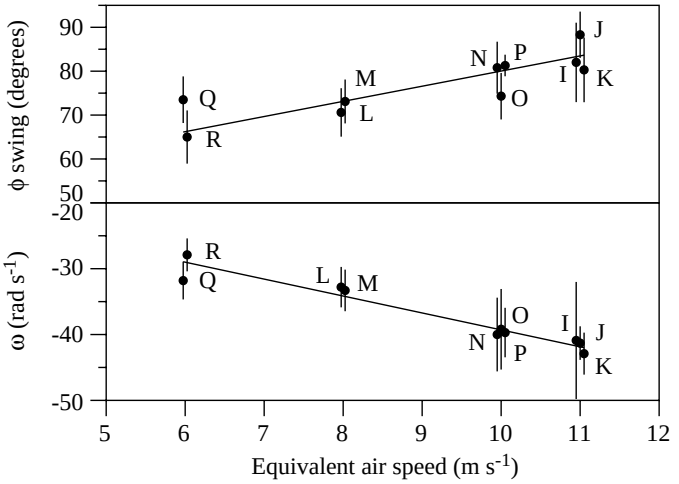

Fig. 7. Upper graph: top-to-bottom swing of humerus angle ϕ within each wing beat in the 10 sequences I–R. Lower graph: peak angular velocity ω during the downstroke (ω is negative because the wing is rotating downwards). The fitted lines are reduced major axis lines, but they have no formal significance. Values are means ± S.D.

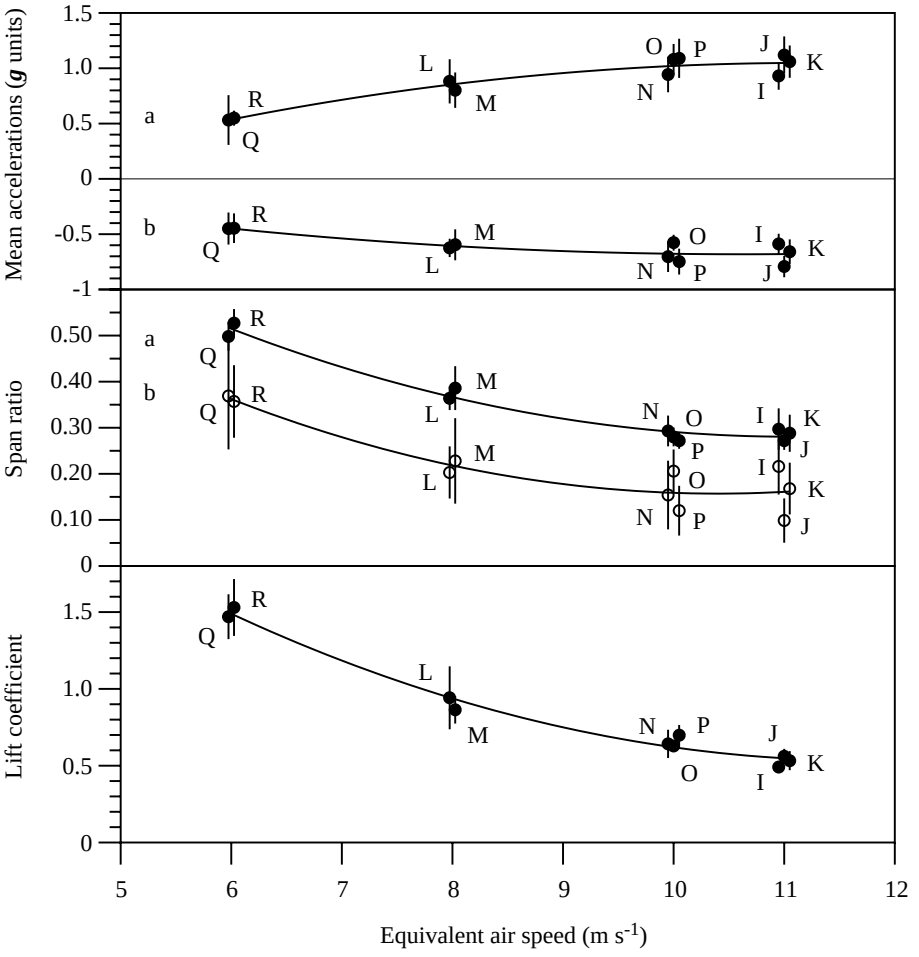

Fig. 8. Top graph: average upward acceleration during the downstroke (a) and upstroke (b) in the 10 sequences I–R. Middle graph: span ratio (a) and force ratio (b). Bottom graph: lift coefficient based on peak angular velocity from Fig. 7. Values are means ± S.D.

of a 'constant-circulation wake', which was first observed by Spedding (1987) in a kestrel, the creation of transverse vortices in the wake can be avoided by shortening the wings during the upstroke by an amount sufficient to keep the lift per unit span constant. In a bird that is creating such a wake, the lift ratio (upstroke:downstroke) would be the same as the span ratio (Pennycuick 1989b). We were not able to measure the lift during the upstroke because of the varying moment arm, but the average upward acceleration gave us an estimate of the upward force on the shoulder joints from equations 4 and 6, and this is related to the lift by equation 7. The curve of upstroke:downstroke 'force ratio' so calculated looks very similar that of span ratio, but is lower down the graph (Fig. 8). In the simplest possible scenario, this would mean that, to maintain a constant circulation, the bird would have to shorten its wings during the upstroke even more than it does. However, the similarity of the two curves suggests that the difference may be due to the somewhat rudimentary nature of the analysis and that, with more information about the vortex wake, it might turn out that the circulation is indeed constant. The strong sweepback of the hand-wing, and consequent very long effective chord when the wing is flexed, may possibly make the wing behave as though it were shorter than it actually is.

Lift coefficient

The highest lift coefficient observed, approximately 1.5 at 6 m s^{-1}, may not be the maximum of which the swallow's wing is capable, but may be compared with a maximum value of 1.6 measured for a gliding pigeon by Pennycuick (1968). If the lift coefficient is near its maximum at 6 m s^{-1}, the swallow could presumably decrease its speed further, by increasing the angular velocity and humerus angle swing, towards the higher values seen at the high-speed end of the range (Fig. 8). Indeed, video sequences were obtained at speeds down to 3.5 m s^{-1}, although they were not long enough or steady enough to be used for the above type of analysis.

Mechanical events within a sequence

The top graph in Fig. 9 is the smoothed recording of humerus angle (ϕ) for sequence 'O' derived from the unfiltered file shown in Fig. 2. The frame numbers represent the data points in the filtered time series at intervals of 8 ms. They run from 1 to 183, instead of 0 to 364 as in Fig. 2, because only the even-numbered frames from the original sequence were used as data points for the Fourier transform. Eight wingbeat cycles were used for the subsequent analysis, the beginning of each cycle being defined as the first point after the humerus angle changed from negative to positive. These points are

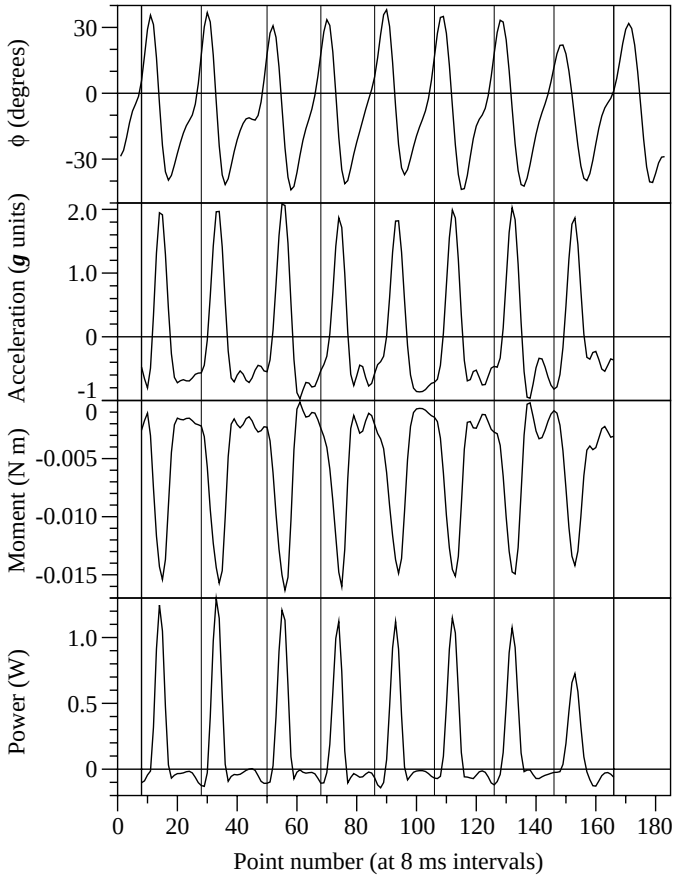

Fig. 9. Top graph: humerus angle for sequence 'O' obtained by low-pass filtering the recording of Fig. 2 from 0 to 21.9 Hz. The thick vertical lines represent the beginning and end of the measurement period, and the thin vertical lines are the boundaries between wingbeat cycles, defined as the first data point after the humerus angle changes from negative to positive. Second graph: vertical acceleration, normalised by dividing by $\boldsymbol{g}$, the acceleration due to gravity. $-1\boldsymbol{g}$ (free fall) is at the bottom of the graph. Third graph: moment applied by the pectoralis muscle to the humerus; values are negative because the moment acts in a downward direction. Zero moment is at the top of the graph. Bottom graph: instantaneous power output of the pectoralis muscles of both sides for each data point.

marked by vertical lines, so that events in the three lower graphs can be correlated with the wing beat.

The second graph in Fig. 9 shows the upward acceleration in '$\boldsymbol{g}$ units', meaning that the acceleration in $\mathrm{m\,s^{-2}}$ has been normalised by dividing it by the acceleration due to gravity ($\boldsymbol{g}$), taken to be $9.81\,\mathrm{m\,s^{-2}}$. The acceleration which the bird 'feels' is 1 unit more than that shown in Fig. 9, because it feels the acceleration due to gravity in addition to the upward acceleration (equation 4). When the upward acceleration is zero, the bird feels $+1\boldsymbol{g}$, as when standing on the ground, while an acceleration of $-1\boldsymbol{g}$ represents the weightless condition or 'free fall'. The peak upward acceleration during each downstroke was approximately $+2\boldsymbol{g}$, which the bird would feel as $+3\boldsymbol{g}$. This is approximately the acceleration experienced by the pilot of an aircraft in a steady, steep turn with 70 ° of bank. The graph indicates that the bird feels the acceleration oscillating over a range of more than $2.5\boldsymbol{g}$ approximately seven times per second – quite a rough ride! The acceleration does not go down as far as $-1\boldsymbol{g}$ during the upstroke (or only momentarily), meaning that the air exerts a net upward force on the wings, throughout the cycle.

The third graph in Fig. 9 is the moment exerted by the pectoralis muscle on the humerus. The moment is negative throughout the cycle, meaning that the pectoralis is pulling downwards. The downward moment during each downstroke, when multiplied by the angular velocity of the wing, gives the instantaneous power output of the muscle. This is plotted (for both sides) in the bottom graph. When this power is multiplied by the interval between frames, it gives the work done in each 8 ms interval. The graph shows a small amount of negative work being done during the upstroke, but the amount shown is based on the same value of the moment arm used during the downstroke. In fact, the wing is drastically shortened during the upstroke, as noted above, and the negative work done would be much smaller than shown. When accumulating the work done in each cycle, we ignored the upstroke and accumulated the work only if the wing was rotating downwards ($\omega<0$). The work done in a given downstroke, when divided by the time for that wingbeat cycle, gives an estimate for the average power output of the muscles in that cycle. Eight such estimates were obtained from sequence 'O', and their mean and standard deviation serve as the average power for the sequence and its standard deviation. Likewise, means and standard deviations for other variables, which could be estimated for each cycle, were the basis of the points and error bars in Fig. 10, in which air speed is the abscissa.

Correction for energy changes

The mean power estimate for each sequence was corrected by subtracting any kinetic energy and potential energy gained during the sequence from the total work done by the muscles. The potential energy correction was always small (see above) but, because of the short duration of the sequences, the gain or loss of kinetic energy could be an appreciable fraction of the measured work done by the muscles. If the speed of the bird is V_1 at the beginning of the sequence and V_2 at the end, then the gain in kinetic energy during the sequence is:

$$\Delta E_\mathrm{k} = m(V_2^2 - V_1^2)/2\,, \qquad (14)$$

but what speed, exactly, is V? At first sight, it appears that a bird flying steadily in the wind tunnel has zero kinetic energy because its ground speed is zero, which is true if we want to estimate the energy that would be dissipated in a collision with the tunnel structure. However, the useful kinetic energy available to the bird is based on its air speed, not its ground speed, and specifically on its true air speed. If we imagine a gull standing on a post with its wings folded, in a wind of, say, $10\,\mathrm{m\,s^{-1}}$, its kinetic energy is not zero, but is based on the square of the wind speed. This energy is real and is available to the bird for immediate conversion into potential energy. If

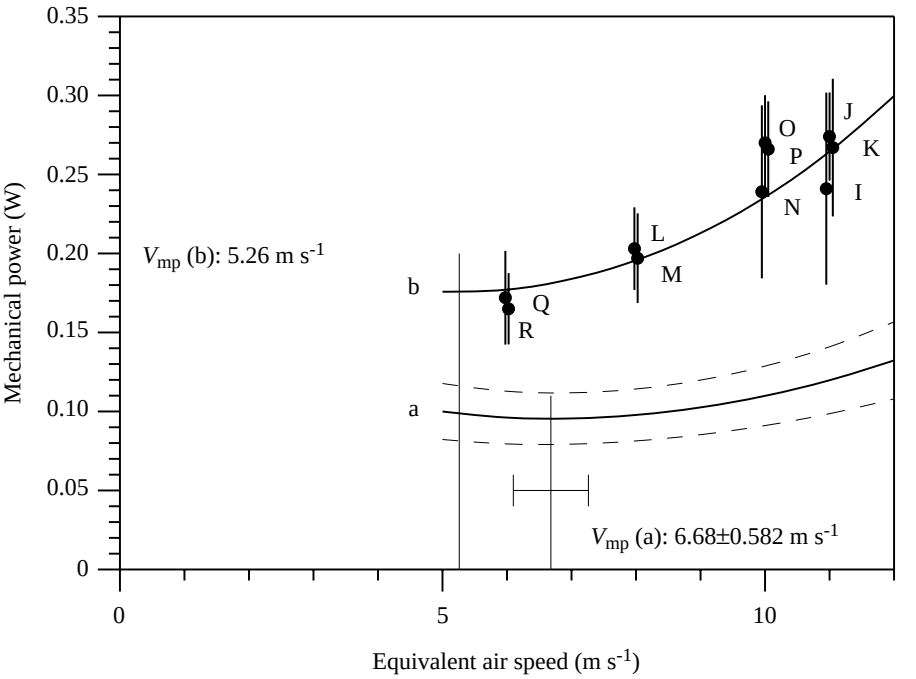

Fig. 10. Average power for the 10 sequences I–R *versus* equivalent air speed. Curve a is the predicted power using currently recommended defaults for body drag coefficient and profile power ratio. Curve b is the predicted power using higher values for body drag coefficient and profile power ratio (see text). V_{mp}, minimum power speed. Values are means ± S.D.

the gull opens its wings, it can climb without doing any muscular work. Its ground speed (backwards) increases if it does this, but its kinetic energy decreases as it climbs because it is losing air speed. If a bird in a wind tunnel increases its speed by muscular exertion, it does so by developing a thrust force against air that is streaming past at the wind speed. The higher the wind speed, the more work must be done for a given gain of speed. Our measurements of muscular work include any work that may be done in increasing the air speed, so we have to measure any gain of kinetic energy, and substract it, to obtain a corrected estimate of the work that would have been needed to maintain a steady speed.

The smoothed value of x for sequence 'O' (Fig. 3) starts at zero at the left-hand edge of the frame. At the beginning of the measurement period (first vertical line), the line slopes downwards, indicating that the bird has a positive ground speed and that its air speed exceeds the wind speed; at the end of the period, the line slopes upwards, indicating that the bird has lost some speed. The true air speed was 10.3 m s^{-1} at the beginning of the sequence and 9.9 m s^{-1} at the end. These are V_2 and V_1 in equation 14. The decrease in air speed means that some of the kinetic energy, built up by muscular exertion before the sequence started, was lost during the sequence. We took account of this energy by estimating it from equation 14 and adding it to the observed work done during the sequence. The correction amounted to approximately 30 % of the muscular work in this particular sequence, although it did not exceed 10 % in any other sequence. It may be noted that we do not need to account separately for the work associated with kinetic energy changes at each wingbeat, because the work done is already included in our estimate of the work done by the muscles, in the same way as the inertial work for accelerating the wings (below).

No correction needed for inertial work

Muscular work is also done to accelerate the wing at the beginning of each downstroke and to put the upward bend in the primary feathers (Pennycuick and Lock, 1976). This work originates from the downward moment applied by the pectoralis muscle to the humerus, multiplied by the downward rotation of the humerus, and is included in the measured work shown in Fig. 9: but what happens to the inertial work at the end of the downstroke? The rotational kinetic energy of the wing (E_{kw}) during the downstroke is given by:

$$E_{kw} = (I\omega^2)/2\,, \qquad (15)$$

where I is the moment of inertia of the fully extended wing and ω is the angular velocity. The moment of inertia is proportional, to a first approximation, to the square of the semispan. This, as noted above, decreases by a factor of more than 3 at the higher speeds, when the wing folds at the end of the downstroke. Therefore I, and the kinetic energy with it, would decrease by an order of magnitude when the wing folds at the end of the downstroke, even if ω were to be maintained at its peak value. We do not know exactly what happens to this energy, but the most likely possibility, which we hope to investigate in the future by simultaneous observations of the vortex wake, is that most or all of it is added to the kinetic energy of the air stream in a way that augments the lift or thrust developed by the wing. There is currently no basis for making an allowance for the wing kinetic energy in the power calculation, because we do not have any reason to assume that any substantial fraction of it is lost.

Mechanical power curve

We can now plot our estimates for the mean power in each sequence, corrected for gains or losses of potential and kinetic

energy, with error bars representing the standard deviation of the power estimates for each wing beat (Fig. 10). Curve 'a' is a power curve from Program 1A of Pennycuick (1989a), using values of C_{Db}=0.1 for the body drag coefficient, and X_1=1.11 for the profile power ratio. The uncertainty boundaries represent ±1 standard deviation, estimated by the physicists' method, by considering the contributions made by each of the variables involved in the calculation to the final power estimate. The body drag coefficient and induced power factor are both assumed to be subject to 20 % uncertainty. On these assumptions, the experimental points are far above the supposed upper limit. Curve 'b', which fits reasonably well through the points, was obtained by increasing C_{Db} to 0.26 and X_1 to 2.25.

Discussion

Anomalously high power estimates

Our power estimates imply that the body and/or wing drag exceeded the values calculated from our assumed values for the body drag coefficient and the profile power ratio. The value of the body drag coefficient (0.26) that generated curve 'b' in Fig. 10 is actually at the lower end of the range used for the original defaults in Program 1A, as published by Pennycuick (1989a). These defaults were revised downwards following the observation by Pennycuick et al. (1996) that the minimum power speeds of two birds, a teal (*Anas crecca*) and a thrush nightingale (*Luscinia luscinia*), were clearly well above the values predicted if C_{Db} was assumed to lie in the original default range 0.25–0.4. However, if a value of C_{Db}=0.1 is substituted, as suggested, and used to calculate curve 'a' for the swallow, the predicted value for the minimum power speed, V_{mp} (6.68 m s^{-1}), is clearly too high. Curve 'b', using C_{Db}=0.26, has a minimum at 5.26 m s^{-1}, which agrees better with the trend of the experimental points. The profile power also had to be doubled, to raise curve 'b' to the level of the points. The distinction is that profile power is assumed to be speed-independent, whereas an increase in C_{Db} increases the parasite power, which is assumed to vary with the cube of the speed. An increase in profile power raises the whole curve without affecting the slope or the value of V_{mp}, whereas an increase in C_{Db} raises the right-hand end of the curve more than the rest and moves V_{mp} to a lower speed. While it is possible that the swallow has a high body drag coefficient, because of the length and area of its tail, the high value of profile power would imply an unexpectedly 'draggy' wing.

We could say that, to make the predicted curve fit the experimental points, we had to add a large amount of drag into the calculation, some of it speed-dependent and some speed-independent, without too explicitly identifying these components with parasite and profile drag. Before too hastily concluding that the values for drag coefficients, measured on frozen bodies by Pennycuick et al. (1988), were right after all, and that our estimate of profile power was far too low, we should consider whether this particular swallow could have been generating extra drag for some reason connected with its behaviour or with the wind tunnel environment. As shown in Table 2, although each of our picture sequences contained hundreds of frames, the measurement intervals were short, ranging from 0.75 to 3.1 s. The bird was not flying steadily, even for these short periods, but was moving its tail and its head, as swallows typically do in manoeuvring flight. In several of the sequences, the tail can be seen to be partially spread, and raised, lowered or twisted, and the bird also often turned its head to one side or the other, sometimes through a large angle. Turning the head would certainly cause additional body drag, whereas use of the tail for manoeuvring would cause additional vortex drag. This is known as 'trim drag' when caused by deflection of the control surfaces in an aircraft and can make a substantial contribution to the total drag. Similarly, spreading and deflection of a bird's tail can have a substantial effect on the total drag in either direction (Thomas, 1996). We might get lower power measurements with birds such as the teal and the thrush nightingale, both of which would fly steadily in one spot for longer periods, without spreading their tails, manoeuvring or moving their heads about.

It is also possible that the minimal amount of turbulence from the net, across the upstream end of the test section, might have modified the flow over the swallow's wings in some way. It may seem unlikely that this would cause a substantial amount of extra drag, but the possibility is interesting because nothing is currently known about the effect of small amounts of turbulence in the air stream on the flow over feathered wings. An experimental approach to this will require a bird that flies sufficiently steadily to be tested with and without an upstream net, under otherwise identical conditions.

Metabolic power

To calculate the rate of consumption of fuel energy from our measurements of mechanical power, some assumptions have to be made about the conversion of fuel energy into mechanical work. This was done in Program 1 of Pennycuick (1989a), but lack of quantitative information in this area means that several of the assumptions are little better than guesswork. In contrast to flight mechanics, there is no coherent body of theory to predict the details of energy conversion. Some gaps that need to be filled were pointed out by Pennycuick (1998b). Notwithstanding this, the stepwise method of calculating performance in long flights, used by Pennycuick (1998a) and based on the same assumptions as Program 1, gives good agreement with observations of the performance of great knots (*Calidris tenuirostris*) migrating approximately 5400 km non-stop from Australia to China, reported by Battley et al. (2000), assuming C_{Db}=0.1 and the profile power ratio X_1=8.4/r, where r is the aspect ratio. These birds would not get even half way to China, under the assumptions underlying curve 'b' of Fig. 10. The default values appear to be realistic for birds that may be presumed to have been flying in an optimal manner because they were observed on long-distance migratory flights. The most likely explanation for the additional drag that we observed here is that the swallow's flight behaviour in the wind

tunnel was less than optimal in respect of drag, rather than that swallows are inherently less efficient than great knots.

Concluding remarks

Our new method for measuring mechanical power is somewhat laborious, and there is scope for improvement in the extraction of kinematic information from the video pictures. However, the reasoning is simple and direct, and the results are internally consistent and credible. The next step is to apply the method to a range of species, and to birds that have been conditioned to fly more steadily, to determine the reasons for the present discrepancy between observed and predicted power. This should provide a much improved basis for determining how the requirement for fuel energy is related to the mechanical power. A future development of the method will be to correlate the analysis of individual wing beats, outlined in Fig. 9, with similarly detailed simultaneous observations of the vortex wake.

We are most grateful to the Swedish Council for Planning and Coordination of Research for a grant for the purchase of the high-speed video system and to the Swedish Natural Science Research Council and Carl Tryggers Stiftelse for support to A.H. We thank Kirsty Park for her help in training the birds, Kenneth Bengtsson for a frozen swallow, Geoff Spedding for helpful comments on a preliminary version of the manuscript, and Thomas Alerstam for his support and encouragement throughout the project.

References

Battley, P. F., Piersma, T., Dietz, M. W., Tang, S., Dekinga, A. and Hulsman, K. (2000). Empirical evidence for differential organ reductions during trans-oceanic bird flight. *Proc. R. Soc. B* **267**, 191–195.

Biewener, A. A., Corning, W. R. and Tobalske, B. W. (1998). *In vivo* pectoralis muscle force–length behavior during level flight in pigeons (*Columba livia*). *J. Exp. Biol.* **201**, 3293–3307.

Biewener, A. A., Dial, K. P. and Goslow, G. E. (1992). Pectoralis muscle force and power output during flight in the starling. *J. Exp. Biol.* **164**, 1–18.

Chatfield, C. (1996). *The Analysis of Time Series* (5th edition). London: Chapman & Hall.

Dial, K. P. and Biewener, A. A. (1993). Pectoralis muscle force and power output during different modes of flight in pigeons (*Columba livia*). *J. Exp. Biol.* **176**, 31–54.

Dial, K. P., Biewener, A. A., Tobalske, B. W. and Warrick, D. R. (1997). Mechanical power output of bird flight. *Nature* **390**, 67–70.

Kirkpatrick, S. J. (1990). The moment of inertia of bird wings. *J. Exp. Biol.* **151**, 489–494.

Pennycuick, C. J. (1968). A wind tunnel study of gliding flight in the pigeon *Columba livia*. *J. Exp. Biol.* **49**, 509–526.

Pennycuick, C. J. (1989a). *Bird Flight Performance. A Practical Calculation Manual*. Oxford: Oxford University Press. 153pp.

Pennycuick, C. J. (1989b). Span-ratio analysis used to estimate effective lift:drag ratio in the double-crested cormorant *Phalacrocorax auritus*, from field observations. *J. Exp. Biol.* **142**, 1–15.

Pennycuick, C. J. (1998a). Computer simulation of fat and muscle burn in long-distance bird migration. *J. Theor. Biol.* **191**, 47–61.

Pennycuick, C. J. (1998b). Towards an optimal strategy for bird flight research. *J. Avian Biol.* **29**, 449–457.

Pennycuick, C. J. (1999). *Measuring Birds' Wings for Flight Performance Calculations* (2nd edition). Bristol: Boundary Layer Publications.

Pennycuick, C. J., Alerstam, T. and Hedenström, A. (1997). A new wind tunnel for bird flight experiments at Lund University, Sweden. *J. Exp. Biol.* **200**, 1441–1449.

Pennycuick, C. J., Klaassen, M., Kvist, A. and Lindström, Å. (1996). Wingbeat frequency and the body drag anomaly: wind tunnel observations on a thrush nightingale (*Luscinia luscinia*) and a teal (*Anas crecca*). *J. Exp. Biol.* **199**, 2757–2765.

Pennycuick, C. J. and Lock, A. (1976). Elastic energy storage in primary feather shafts. *J. Exp. Biol.* **64**, 677–689.

Pennycuick, C. J., Obrecht, H. H. and Fuller, M. R. (1988). Empirical estimates of body drag of large waterfowl and raptors. *J. Exp. Biol.* **135**, 253–264.

Spedding, G. R. (1987). The wake of a kestrel (*Falco tinnunculus*) in flapping flight. *J. Exp. Biol.* **127**, 59–78.

Spedding, G. R. and Lissaman, P. B. S. (1998). Technical aspects of microscale flight systems. *J. Avian Biol.* **29**, 458–468.

Thomas, A. L. R. (1996). Why do birds have tails? The tail as a drag reducing flap and trim control. *J. Theor. Biol.* **183**, 247–253.